



Effect of Cooling Rate on the Oleogel Properties of Wax–Wax-Hydrolyzate Mixtures

Till Wettlaufer¹ · Eckhard Flöter¹

Received: 6 December 2021 / Accepted: 17 February 2022 / Published online: 16 March 2022
© The Author(s) 2022, corrected publication 2022

Abstract

In this contribution, the effect of cooling rates on a wide compositional range of waxes as oleogel structurants was systematically investigated. The different waxes exhibited varying levels of wax esters (WE), fatty acids (FA), fatty alcohols (FaOH) and hydrocarbons (HC) and were systematically altered by combinations of sunflower wax (SFW), bees wax (BW) and their hydrolyzed variants (SFW_h, BW_h). By applying slow, medium and high cooling rates, the resulting gel properties were investigated in terms of firmness, calorimetry and microstructure. It was found that the calorimetric signal is mainly affected by the waxes' composition. However, due to enlarged dynamic induction times upon crystallization, a shift in dissolution temperature could be observed in heating scans. In our latest work we were able to formulate the degree of homogeneity (DoH), with which it was possible to predict the undercooling in SFW mixtures. The introduction of a novel method emerged for firmness measurements of oleogels treated with the different rates. Thus, it was possible to detect with high sensitivity for all waxes for applied cooling rates, caused by modification of microstructure. Combination of different methods further elucidated that higher rates need to be applied to further scale firmness of oleogels in industrial processes.

Keywords Wax · Oleogel · Cooling rate · Firmness · Sunflower wax · Bees wax

Introduction

Conventionally semi-solid lipid phases are structured by high melting triacylglycerides (TAGs). Oleogels, non-TAG structured lipid phases, are an alternative that offers the benefit of lower levels of saturated and *trans* fatty acids [1, 2]. Even though not yet extensively introduced into the market, they are considered as an attractive alternative to conventional fat phases and might inspire consumer-oriented product designs.

Among others, waxes have been proven to be a very auspicious group of oleogelators [3, 4]. This is mainly due to their low inclusion levels, low costs and potentially broad availability. Their acquisition is essentially based on purification, such as the winterization of oils, which distinguishes them from other oleogelators, which in contrast, are obtained through sophisticated modification processes. In addition, some waxes have already been approved as food ingredients by the FDA

and EFSA, although for now only as glazing and coating agents. This facilitates future market introductions. The term wax covers a huge variety of materials since waxes consist of different mixtures of hydrocarbons (HC), wax esters (WE), fatty acids (FA), fatty alcohols (FaOH) and other minor components. Each of those major components, is able to structure liquid oils independently [5–7]. However, each class of molecules again covers a range of different chain lengths. In 2017, Doan et al. [8] analyzed different waxes diligently, delivering a comparative insight into wax compositions. However, the exact composition of the waxes is difficult to determine, as the analytical methods are not standardized and the available waxes are subject to natural variations and different purification processes used by producers.

Due to their multicomponent character, different combinations of waxes and solvents exhibit substantial differences in gel characteristics. Recent contributions illustrated this property [9, 10], disclosing the effect of minor components and oil type on oleogels based on combinations of different waxes with either sunflower-, canola- or MCT-oil. A wide range of differences were found, from critical gelling concentration (CGC), thermal behavior to macroscopic oleogel properties like firmness.

✉ Till Wettlaufer
till.wettlaufer@tu-berlin.de

¹ Faculty III Process Sciences, Department of Food Technology and Food Chemistry, Food Process Engineering, Technische Universität Berlin, Berlin, Germany

These compositional qualities, affecting the gel properties, are complemented by applied processing conditions. In a comprehensive review, Doan et al. [3] demonstrated how both internal and external factors affect wax-based oleogels. External factors considered in that contribution were primarily cooling rate and shearing. Well-established for crystallization, and TAG crystallization in particular, both external factors influence nucleation and crystal growth substantially. Altering these hence allows to manipulate the properties of the final network structure. In the field of wax-based oleogels, it is known that the cooling rate has a crucial impact on the gel properties [11]. Furthermore, it seems to be generally acknowledged that an improved oil binding capacity (OBC) and a higher gel hardness can be obtained by tailoring the crystal network [12, 13]. Most of the studies investigated the influence of cooling rates by the application of straight waxes. It should be noted that it was reported that the gels induced by slower cooling rates reveal higher gel-sol transition temperatures [14].

In multicomponent waxes, the effects induced by the different chemical species are possibly independently superimposed or subject to detailed molecular interactions [7, 15]. In an earlier contribution of ours, oleogels based on combinations of SFW, BW and their hydrolyzed versions were studied [16]. This study covered an extended compositional range and revealed the occurrence of multiple coexisting solid phases as a function of composition. Throughout the different experiments of this study, the cooling rate was deliberately kept constant at 5 K/min to ensure a limited influence of external factor variations. From fat crystallization it is known that the apparent mixing behavior is subject to variation of the cooling rate [17]. However, the use of a broad and strongly differentiated compositional framework of waxes allows to better understand the relationship between wax composition and functionality.

In this work we investigated how vastly different cooling rates, fast (20 K/min), medium (3 K/min) and slow (0.1 K/min), influence the mixing behavior of the compositionally wide ranging mixtures. This further is aiming to illustrate how this propagates into the gel characteristics. The predominantly used concentration of the structurants is chosen fairly high (16% w/w) in this work, to ensure a reliable collection of data over the whole composition and process range studied. Through application of different cooling rates to the systems studied, we aim to contribute to the elucidation of the interplay of internal and external factors in wax-based oleogels.

Materials and Methods

Materials

Canola oil (refined) was contributed by Gustav Heess GmbH (Leonberg, Germany). Polarity of the oil (4,6% total polar

compounds) was determined by Testo 270 cooking oil tester (Testo SE & Co. KGaA, Titisee-Neustadt, Germany). The fatty acid composition was determined according to DFG method C-VI 10a and is reported in our previous work [16]. Sunflower wax (6607L, Lot.nr. F1911020-001) (SFW), beeswax (8108LM, Lot.nr. F1727017-001) (BW), sunflower wax-hydrolyzate (6607H, Lot.nr. F1637034-001) (SFW_h) and beeswax-hydrolyzate (CERA H, Lot.nr. F1746044-001) (BW_h) were kindly supplied by Kahlwax GmbH & Co KG (Trittau, Germany). All materials were used without further modification or purification.

Figure 1 illustrates the composition of the obtained wax-wax hydrolyzate mixtures. Hydrolysis up to a residual wax ester content of 20% gave rise to waxes of very different composition in the mixtures. These systems exhibit varying wax ester contents (I) and high contents of FA and FaOH (II). It was further reported, that ratio dependent interactions between FA and FaOH occur [7, 18, 19].

In another contribution of ours, we introduced the so-called Degree of Homogeneity (DoH) to better characterize differently composed waxes in terms of their wax ester quantity and quality [10]. This was primarily done since the wax esters are thought to be the most important major components contributing to network formation.

$$DoH = \frac{x_{WE}^2}{\sum(x_n^2)} \cdot \frac{100}{\Delta CN_{WE} + 1} \quad (1)$$

$$\Delta CN_{WE} = CN_{max} - CN_{min} \quad (2)$$

The DoH (Eq. (1)) in essence magnifies the effect of wax ester quantities and incorporates the chain length difference and position of ester bonds within the wax ester species as the chain length disparity, ΔCN_{WE} (Eq. (2)). There, CN refers to the maximum and minimum reported chain lengths of the wax esters. The calculated DoH values were obtained from reported wax compositions by Doan et al. [8].

Oleogel Preparation

Oleogels were produced by crystallization of the wax-structurant in canola oil. The canola oil was heated up to 90 °C on a heating plate with a magnetic stirrer (200 rpm) (MR Hei-Tech, Heidolph Instruments GmbH & Co.KG, Schwabach, Germany). After reaching 90 °C, the wax was added so that a concentration of 16% w/w was yielded. This relatively high inclusion level was chosen, to establish a clear signal throughout the experimental design. However, the mixture was kept isothermal at 90 °C for 30 min to allow complete dissolution. The solution was filled in 5 ml reaction vials (3 ml dosage) and crystallized according to the experimental setup.

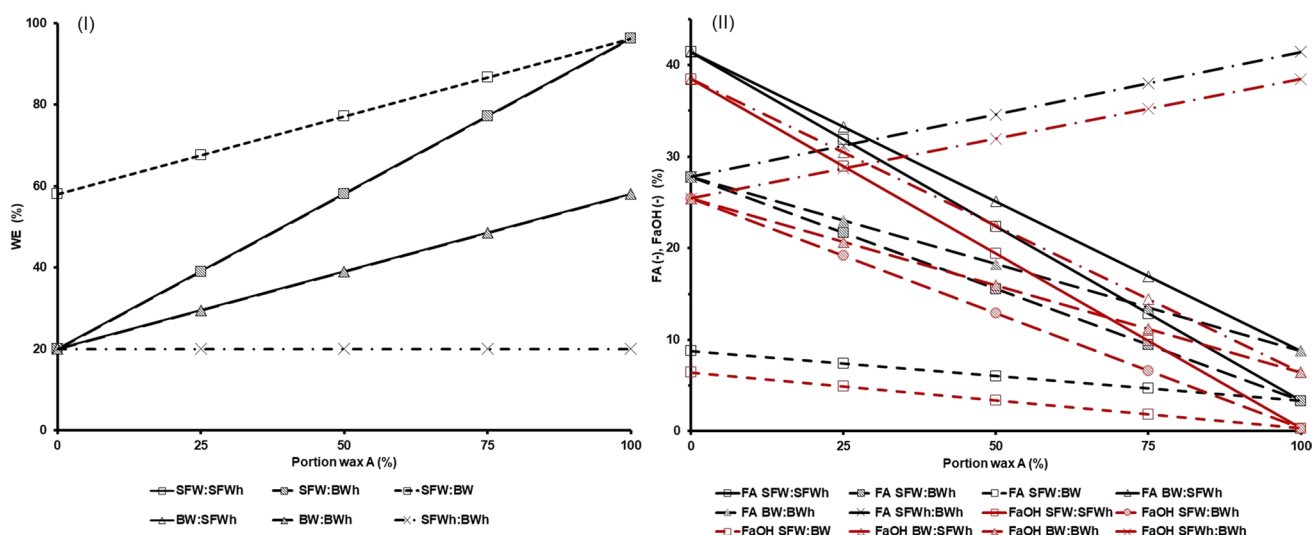


Fig. 1 Computed frequency of wax esters (I) as well as fatty acid (FA) and fatty alcohol (FaOH) (II) portions as a function of mixing ratio based on the reported data by Doan et al. [8]. The x-axis of (I) and (II) refers to the portion of the first mentioned wax in bi-wax mixtures (A:B)

Cooling Rate Experiments

The cooling rates were achieved using a double-jacketed vessel as a silicone oil bath (500 ml, Type 47 V 350, VWR, Germany). The vessel had an inner diameter of 10 cm and was flushed with temperature-controlled silicone oil. An inserted angled blade stirrer (200 rpm) deliberately delivered sufficient heat transfer. The flushed silicone oil was heated and cooled by a thermostat (Unistat Tango, Peter Huber Kältemaschinenbau AG, Offenburg, Germany).

To start the treatment, the silicone oil bath was preheated to 90 °C. The hot samples (wax solutions in vials, see section oleogel preparation) were immersed in the silicone oil bath. A sample holder construction ensured that the entire sample was immersed in the silicone oil bath. After 30 min of stabilization at 90 °C, the batch was cooled at the respective cooling rate to 20 °C. This approach allowed to apply cooling rates of 20 K/min, 3 K/min and 0.1 K/min which were chosen as fast, medium and very slow crystallization rates to mimic possible cooling rates occurring in industrial processes. Prior analysis of crystallized oleogels under quiescent conditions (not immersed in silicon oil) resulted in a determined cooling rate of 1.6 K/min. Every experiment was carried out in six-fold (independent vials). Additional to the monitoring of the silicon oil bath temperature, one sample was temperature monitored with a thermal data recorder (TC08, OMEGA Engineering, Inc., United Kingdom) inserted into the center of sample to verify the accomplishment of the respective cooling rate. Crystallized samples were stabilized for 24 h prior to any analysis at room temperature.

Thermal Behavior in DSC

Differential scanning calorimetry (DSC) was carried out using a 214 Polyma (Netzsch, Selb, Germany) calorimeter. The sample size was 10 ± 1 mg. The crucibles were heated up to 105 °C (5 K/min) and kept isothermal for 10 min. The samples were then cooled to 5 °C with predefined rates. Following a stabilization at 5 °C for 2 min, the samples were heated up to 90 °C with a scan rate of 5 K/min. Each sample was processed in three cycles of cooling and heating. Cooling was performed with 20 K/min, 3 K/min and 0.1 K/min while heating was always carried out with 5 K/min. The heat of dissolution (can be regarded in the following similar to the ‘heat of fusion’), the dissolution offset ($T_{D,offset}$) and the crystallization onset ($T_{c,onset}$) were determined using Netzsch Proteus® software (Netzsch, Selb, Germany). The dynamic induction time was calculated based on the crystallization onset temperature and the rate applied respectively. Undercooling was calculated according to Eq. (3). For each composition three independent samples were used.

$$\text{Undercooling} = T_{D,offset(0.1K/min)} - T_{c,onset(n)} \quad (3)$$

To elucidate the solubility of the waxes in the oil, the heat of dissolution was determined for 4, 8, 12 and 16% w/w wax inclusion levels. This was done to allow reliable extrapolation to the wax concentration for the value 0 J/g. The stabilized samples (48 h) were measured by heating from 5 °C to 90 °C with a scan rate of 5 K/min respectively.

Microscopy

Brightfield light microscopy (BFM) images were taken using an Axio Scope.A1 KMAT (Zeiss, Jena Germany) combined with an AxioCam ICm1 Rev.1 camera (Zeiss, Jena Germany). The sample preparation for microscopy was in essence as described above. In order to avoid crystal aggregate superposition at high wax concentrations (16% w/w) in the micrographs, a lower wax concentration of 12% w/w was utilized. A hot drop of solution was placed on a preheated (95 °C) glass slide. After the cover glass was administered, the samples were crystallized for one hour on a wooden plate. In order to adjust the focus depth, the crystallized samples were placed under the microscope and then heated to 90 °C by a peltier plate. The gels were stabilized for 30 min to prevent memory effects. Subsequently, cooling ramps were run according to the experimental setup down to 15 °C. Unless otherwise stated, the images displayed are taken at 15 °C.

Firmness

The reaction vessels with samples cooled at different rates were decapitated with a fine saw after 24 h of stabilization. A sample holder always guaranteed the same cut-off height. After cleaning the decapitated vessels with a scalpel, the samples were extruded with a Texture Analyser (Stable Micro Systems, United Kingdom) and a mounted sample holder, see Fig. 9A. A customized geometry ($\varnothing = 10$ mm) was driven into the reaction vessel up to the trigger force (0.02 N). Then exactly 10 mm piston movement extruded the sample at the bottom end. This was done to apply to all systems a defined pressure. The sample was cut off at the open end of the vessel with a scalpel. A collection plate ensured the same sample position after the extrusion of the

oleogels and ensured an easy transfer to the universal testing machine for compression tests.

The final firmness measurements (compression) were performed with a zwickiLine universal testing machine from Zwick Roell (Ulm, Germany) equipped with a 1 kN load cell (trigger force 0.02 N). The 10 mm thick samples were compressed with a 30 mm diameter stainless steel cylinder at 150 mm min⁻¹.

Statistical Analysis

One-way ANOVA with tukey mean value comparison ($p = 0.05$) was carried out using Origin Pro 9 (OriginLab, Northampton, MA, USA).

Results and Discussion

Thermal Behavior

The dosed concentration of 16% w/w is not identical to the level of solid material present in the gels due to solubility of wax components in the liquid oil. To assess the level of solid wax present, an important parameter to derive network effectiveness, it is useful to determine the wax solubility. Figure 2 shows the amount of dissolved material determined by linear extrapolation of the heat of dissolution data for 4, 8, 12 and 16% w/w wax oleogels to 0 J/g. This value indicates a wax concentration without any solid wax present. These gathered values reflect the solubility at the storage temperature. This is hence the minimum concentration for crystallization and per definition lower than the critical gelation concentration (CGC).

Figure 2, left illustrates how partially replacing SFW with either BW (black pattern), SFWh (dark grey) or BWh (light

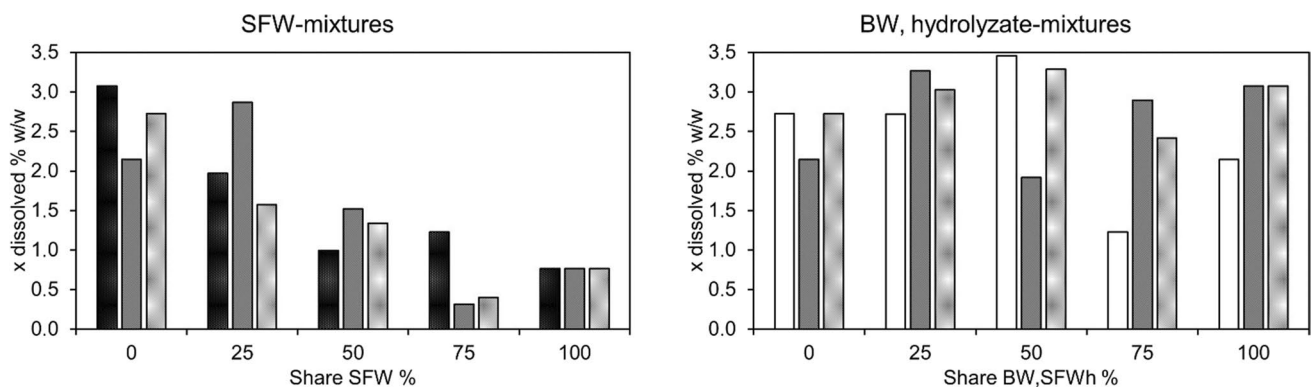


Fig. 2 Dissolved material as a function of mixing ratio. Dissolved material was calculated by heat of dissolution extrapolation ($y = 0$ J/g) based on different levels of wax concentration. Left: SFW-mixtures with SFW-share on x-axis. Second component from left to right: BW, SFWh, BWh. Right: BW- and SFWh-mixtures. BW pro-

portion increases according to x-axis. Dark pillars: mixtures with SFWh. Grey pillars: mixtures with, BWh. White pillars: mixture of SFWh:BW, SFWh proportion on x-axis. Samples were stabilized for 48 h

grey) changes the amount of dissolved wax at 20.5 °C. On the right side of the scale (SFWh-mixtures), the three series end with pure SFWh having a low solubility. The analysis performed shows that the lowest solubilities for mixtures of SFWh with hydrolyzed wax are found in the 75:25 mixing ratio. The right graph depicts the amount of dissolved material for mixtures of BW with the hydrolyzed waxes (SFWh: dark grey; BWWh: light grey) and mixtures of the two hydrolyzed waxes (SFWh:BWWh, white). Here, no clear trend could be identified. Most data hover around a value of 2.5%. The mixture of 75:25 SFWh:BWWh appears to have the lowest solubility value of this series (1.2%).

The heating thermograms of the 16% w/w oleogels are depicted in Fig. 3. The samples were crystallized with different cooling rates and briefly stabilized (see method description above) prior to heating. The curves are differentiated according to the prior applied cooling rate by solid (20 K/min), grey (3 K/min) and dashed lines (0.1 K/min).

The complex dissolution behavior of the wax structurants reflects the multicomponent character with co-existing solid phases. A detailed discussion on this topic can be found elsewhere [16]. For the differentially crystallized samples, it is found that as the cooling rate decreases, the complexity of the phase behavior becomes more pronounced.

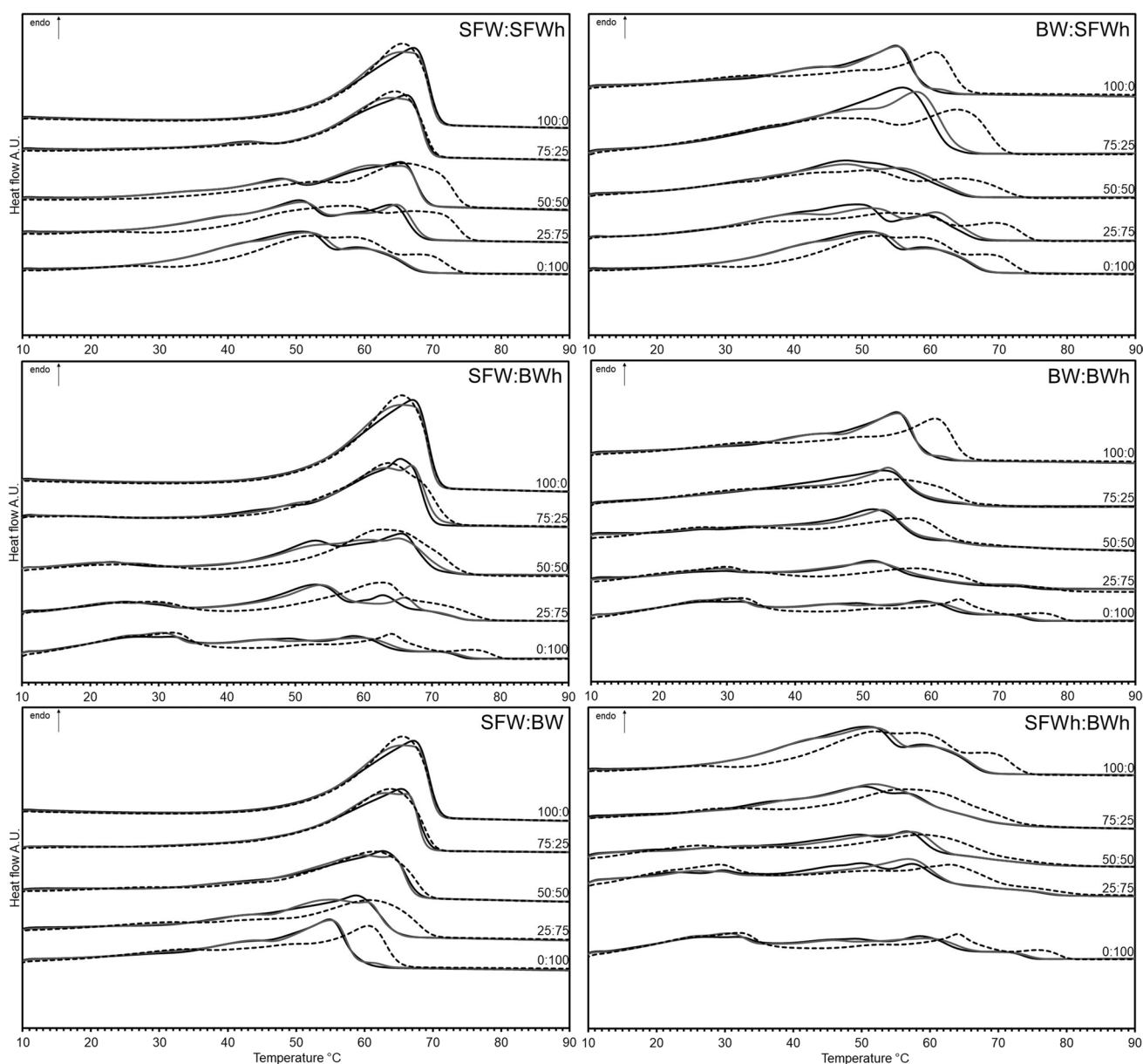


Fig. 3 Average heating thermograms ($n=3$) of 16% w/w oleogels with varied wax composition after previously performed cooling with rates of 20 K/min (black solid lines), 3 K/min (grey solid lines) and 0.1 K/min (black dashed lines). Stabilized at 10 °C for 2 min

SFW (Fig. 3, upper left) exhibits similar responses in the heating scans almost irrespective of the different cooling rates, 20 K/min, 3 K/min and 0.1 K/min. The two higher cooling rates do also not yield any significant differences for the mixtures of SFW and SFWh. Crystallizing at a cooling rate of 0.1 K/min, however, seems to stimulate separate crystallization. The peaks appear to be more segregated and the highest dissolution temperatures are significantly increased. Since SFW is predominantly composed of wax esters, known as the highest melting species in these mixtures, it is surprising to find the highest dissolution temperatures in the intermediate compositions range (SFW:SFWh 50:50). The possible explanations for this phenomenon as for example formation of a compound or demixing of a specifically high melting wax ester mixture, certainly demand further attention. The general pattern of increased segregation with higher dissolution temperature at very low cooling rates is also found for the other gels with mixed structurants containing SFW.

Considering structuring systems based on BW and hydrolyzates, right column in Fig. 3, it is again found that the cooling rates of 20 and 3 K/min deliver insignificantly different heating thermograms. However, different to SFW the crystallization of straight BW appears to be quite sensitive to very low cooling rates. The higher dissolution temperature found for the cooling rate of 0.1 K/min indicates a clear solid segregation of high melting material. This is most likely attributed to mixed wax esters. On admixing SFWh, the dissolution temperature of the slowly crystallized samples increases even further. This is not the case in mixtures of BW and BWh. Only when BWh is the main component, higher dissolution temperatures occur at slow cooling rates similarly to the straight application of BWh.

Also for the combination of both hydrolyzates (SFWh:BWh) only minute changes in the dissolution behavior occur when gels are induced by either cooling down with 20 K/min or 3 K/min. Crystallized at the lowest cooling rate (0.1 K/min) the complicated dissolution behavior is again shifted to higher temperatures.

As described in Table 1, the dynamic induction times are significantly longer at lower cooling rates. This seems to favor less imperfect crystallization. Higher cooling rates possibly kinetically drive integration of molecules into the crystal lattice creating sub-optimal, non-equilibrium mixed crystals. These kinetically induced crystals have as thermodynamics dictate a lower melting point as the thermodynamically stable mixed crystals. This is line with the works on kinetic phase diagrams [20].

The conclusion that the higher dissolution temperature is a result of sub-optimal crystal packing is on the other hand not supported by the assessment of the enthalpy of dissolution. The heat of dissolution data is tabulated in the supplementary data (SI 3) and does not indicate a systematic

change as a function of the cooling rate. An alternative explanation for the higher temperatures observed in the heating thermograms is based on the different size of crystal or crystal agglomerates. As Fig. 7 reveals, the low cooling rate is clearly associated with larger crystalline objects. During temperature scans at constant heating rate, the larger crystal sizes might dictate an apparent slower dissolution rate and hence by means of a time–temperature correlation falsely indicate a higher dissolution temperature. The formation of denser, more thermo-resistant polymorphs under low cooling rates cannot be excluded either. The constant heat of dissolution values as a function of cooling rate, however, do not show any differences, which is why polymorphism is considered as unlikely. However, with the current level of evidence, this interpretation remains wide open for debate.

The cooling thermograms (SI 1 and 2) show essentially that at lower cooling rates the crystallizations starts at higher temperatures, which is already expressed in Fig. 5. Figure 4 exemplarily illustrates the crystallization of gels based on mixtures of BW:SFWh cooled down with different rates.

First, differences in behavior between samples on high (20 K/min, black line) and medium cooling rates (3 K/min, grey line) are more pronounced than in the heating scans of these samples. At the lowest cooling rate studied (0.1 K/min), peaks generally expand over smaller temperature ranges and are more pronounced. This indicates more defined crystallization events and lower probabilities of kinetically induced co-crystallization. This is most apparent by comparing the thermograms for the 50:50 mixture.

The undercooling of the 16% w/w wax solutions was computed as the difference of dissolution offset and crystallization onset (see Eq. (3)). This approach is due to the challenges posed by the complex melting behavior of the various wax mixtures.

Figure 5 shows the undercooling values determined as a function of wax composition and cooling rate. Throughout the samples it is valid, that the undercooling increases from 0.1 K/min (white pillars) to 3 K/min (grey pillars) and 20 K/min (black pillars). Further, it is noticeable that all mixtures with SFW exhibit lower undercooling values with increasing concentrations of SFW. This is in line with an earlier contribution of ours. Waxes with a high degree of homogeneity (DoH, see also Eq. (1)), hence high amounts of wax esters homogeneously distributed, showed lower undercooling [10]. In addition, the wax ester chain length disparity (Eq. (2)) increases when two waxes of different origin (SFW and BW) are mixed, which is also expressed in increased DoH values. For the wax mixtures systematically modified in this contribution, the DoH are shown as a circles (O), which relate to the right y-axis in Fig. 5.

As mentioned before, mixture of two different wax ester species leads to lower DoH values. This is explicitly visible by comparing the data obtained for SFW:SFWh and

Table 1 Dynamic induction times (minutes) of oleogels (16% w/w) cooled at different rates

Wax A	SFW	Wax B	SFWh	Share A (%)	Share B (%)	25	50	75	100	BWh	25	50	75	100	BW	25	50	75	100	
0.1 K/ min	175.0±0.03	132.7±0.01	100.7±0.01	38.33±0.01	36.0±0.02	173.67±0.02	99.33±0.07	68.67±7.37	36.00±0.02	134.67±0.01	107.67±0.00	61.00±0.02	44.67±0.02	36.00±0.02						
3 K/ min	6.19±0.16	4.63±0.09	3.44±0.02	1.40±0.03	1.37±0.03	8.84±0.12	6.34±0.08	4.08±0.48	2.64±0.46	1.37±0.03	3.88±0.02	2.21±0.05	1.78±0.13	1.37±0.03						
20 K/ min	1.01±5.20	0.78±2.31	0.61±0.58	0.30±1.15	0.31±1.73	1.42±1.73	1.09±7.757	0.72±8.39	0.52±0.05	0.31±1.73	0.70±1.53	0.46±1.73	0.36±3.79	0.31±1.73						

Wax A	BW	Wax B	SFWh	Share A (%)	Share B (%)	25	50	75	100	BWh	25	50	75	100	SFWh	BW	25	50	75	100	
0.1 K/min	175.00±0.03	204.33±0.02	223.33±0.02	148.00±0.01	134.67±0.01	307.00±0.02	312.33±0.14	214.67±0.01	134.67±0.01	215.00±0.02	295.00±0.05	233.67±0.05	203.00±0.00	175.00±0.03							
3 K/min	6.19±0.16	7.34±0.12	8.38±0.16	6.24±0.05	4.99±0.05	10.34±0.12	10.84±0.93	8.06±0.08	4.99±0.05	8.84±0.12	10.43±0.23	8.57±0.29	7.22±0.05	6.19±0.16							
20 K/min	1.01±5.20	1.15±6.43	1.41±12.66	1.03±1.00	0.89±1.53	1.65±4.00	1.73±29.67	1.30±8.74	0.89±1.53	1.42±2.65	1.62±7.57	1.36±9.24	1.15±2.00	1.01±5.20							

Cells contain mean values and errors as standard deviation respectively

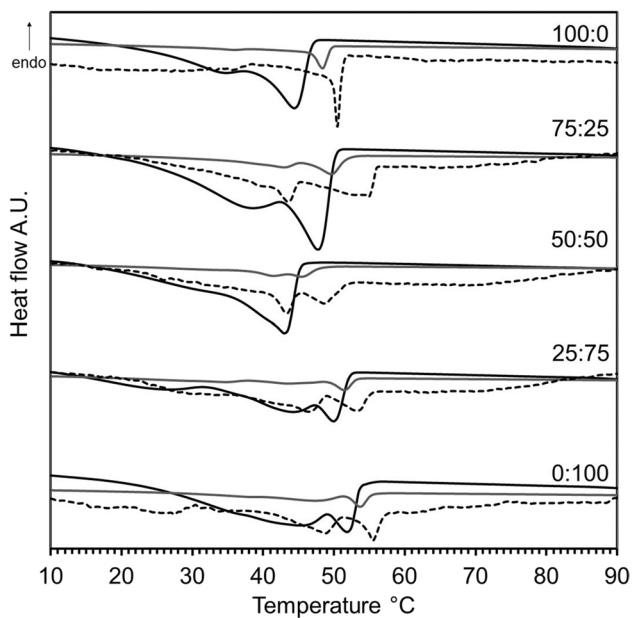


Fig. 4 Cooling thermograms of 16% w/w oleogels (BW:SFW). 0.1 K/min=dotted line, 3 K/min=grey line and 20 K/min=black line. Scans at 0.1 K/min are scaled differently for visibility

SFW:BWh mixtures. The image becomes more complicated considering mixtures of BW with either SFWh or BWh. Despite the fact that the DoH increases systematically with BW inclusion levels, the highest undercooling is at intermediate compositions. For mixtures of the two hydrolyzates, the DoH remains low and offers little insight. The undercooling observed for SFWh gels is similar to the one observed for BW, while BWh gels show higher undercooling. By linear fitting of the DoH *versus* undercooling data of different waxes obtained from our recent study [10], the undercooling could be predicted quite well for the systems investigated in this work. The predicted values are illustrated as triangles (Δ) in Fig. 5. It should be noted that the correlation used is based on data taken at another scan rate (5 K/min). Nevertheless, as the results in Fig. 5 reveal, undercooling is less sensitive to variations in cooling rate than to variations in composition in the ranges studied. Attempts to correlate the undercooling with the amount of dissolved material did not deliver any meaningful results (not shown).

The kinetics of crystallization remains difficult to characterize. Obviously, the detection of initial crystals resulting from the interplay of nucleation and growth rate is a function of the sensitivity of the detection method. Even though undercooling as a function of cooling rate, is well defined compared to for example induction time, it ignores kinetics somehow. To reflect that different cooling rates are associated with different times in the undercooled state, the dynamic induction times were calculated. These were derived from the undercooling data collected when different

cooling rates were applied. The durations of supersaturation until the appearance of crystallization are given in Table 1. Not surprisingly, the general pattern within a series of different mixtures, revealed in Fig. 5, propagates directly into these data.

In line with Fig. 5 the data show that increasing cooling rates relate to shorter dynamic induction times. Extremely low rates of 0.1 K/min however, result in induction times ranging from 312 to 36 min. In contrast to that, 3 K/min and 20 K/min cause induction times in the ranges of 10 to 1.37 min, and 1.73 to 0.3 min, respectively.

From all waxes used in the experimental design, SFW shows the shortest induction times. Straight BW has irrespective of the cooling rate about four times as long dynamic induction times as SFWh. Among the hydrolyzed waxes, SFWh is crystallizing faster than BWh, approximately 15% and 50% slower than BW, respectively.

Regarding the specific dynamic induction times of individual wax mixtures, it becomes obvious that mixtures with increasing level of SFW show the lowest induction times. The induction times of the SFW-containing mixtures evolve in general systematically with the dynamic induction times of the components admixed: BWh slowest, SFWh intermediate and BW least slow. BW based mixtures with either SFWh or BWh yield longer dynamic induction times than the SFW systems. Different to the SFW-based mixtures, those based on BW show longest dynamic induction times in the intermediate mixing range. This is also true for the mixtures of the two wax hydrolyzates (SFWh:BWh). The overall pattern found, however does not correspond to the DoH or the amount of dissolved wax.

Microstructure

To further study the effect cooling rate variation, the microstructure of oleogel solutions crystallized on glass slides was studied. The microstructure can provide helpful information in the assessment of the macroscopic properties of the gels such as firmness, oil binding capacity or rheological behavior [13].

Building on the discussion above, Fig. 6 combines cooling thermograms and images of crystallization events. The four wax-based gels displayed in the figure were obtained by 12% w/w oleogels. The images and thermograms relate to a cooling rate of 0.1 K/min.

In the initial stages of SFW crystallization (top row), platelet-like aggregates grow orthogonal to the view of sight (Event 1). This seems to be primarily due to observations that are typical of SFW. However, the interpretation of needle-like SFW-crystals has already been declared an artifact or growth orientation [21, 22]. The platelet-like appearance also corresponds to observations made for pure wax esters [23]. With ongoing cooling, a shoulder in the thermogram

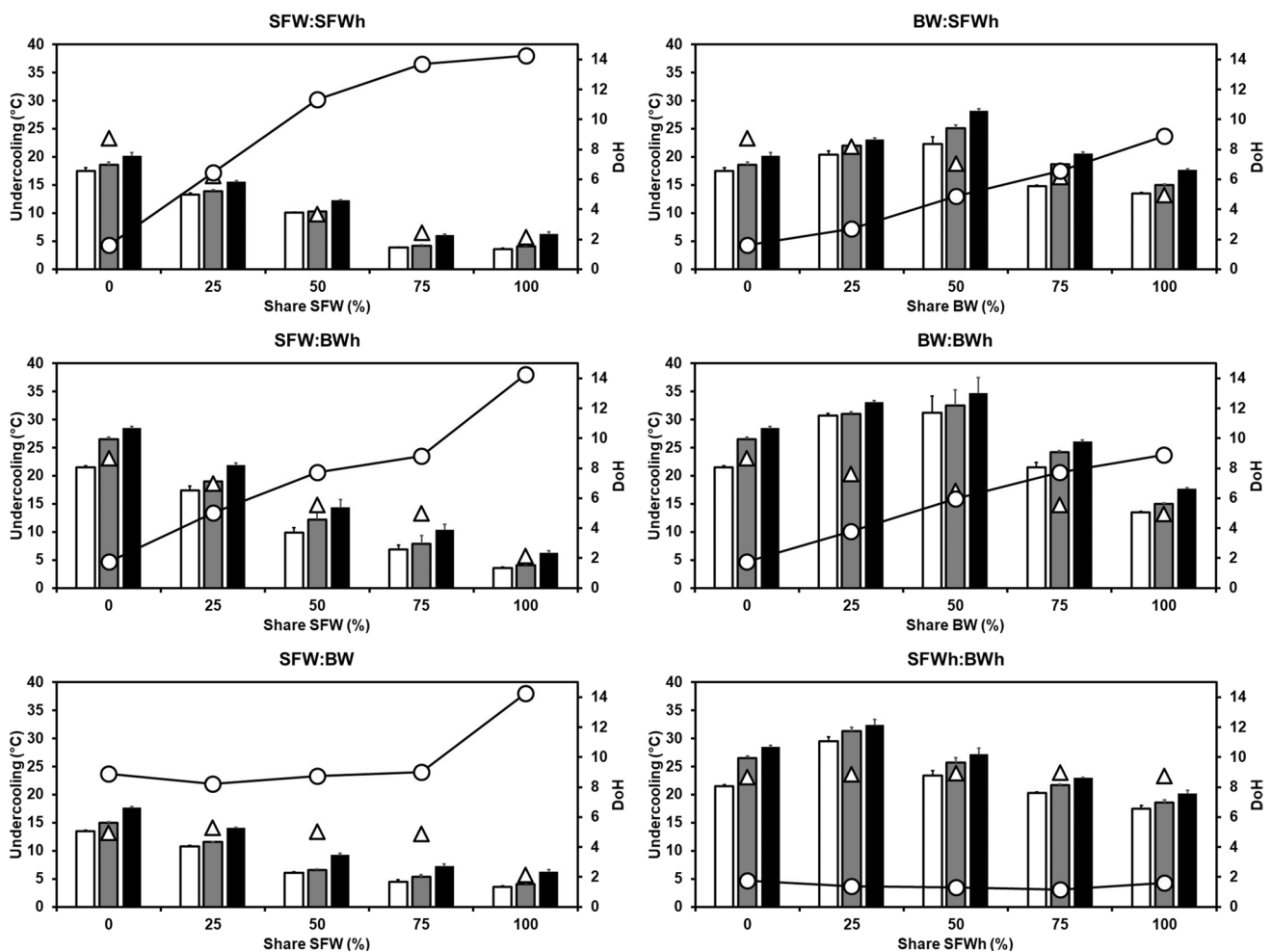


Fig. 5 Undercooling of 16% w/w oleogels ($n=3$) treated with 0.1 K/min (white pillars), 3 K/min (grey pillars) and 20 K/min (black pillars) as a function of wax composition. The computed degree of homogeneity (DoH) of the waxes is depicted as circles (O) for the mixtures. Further, the predicted undercooling based on DoH-Undercooling of different natural waxes is depicted as triangles (Δ)

appeared and is accompanied by the occurrence of a more feathered type of crystal aggregates (Event 2). Since SFW consists of 96% wax esters with chain lengths ranging from 44–50, the two events possibly relate to changes in the wax ester crystallization. Initially, only highest melting longer chain wax esters crystallize which are accompanied by another fraction of wax esters at lower temperatures. If this sequential crystallization results in a mixed crystal with temperature dependent composition gradients, or a second solid phase, remains unresolved here.

SFWh in contrast shows spherulitic aggregates. The existence of spherulites is based on poly-nuclei, poly-impurities or split growth [24]. In other words: numerous crystal orientations grow from a central nucleation point, developing more dendritic structures, forming a spherulite. Taking the thermogram of SFWh into account, two events are clearly identifiable with an additional shoulder. Combining this with the micrographs obtained, it seems fair to assume that the

growth of the initial spherulite relates to the first peak. The compaction of the outer of the spherulite is possibly related to the shoulder (Event 2). The loosely packed crystals on the spherulites' surface may be referred to the distinct second peak (Event 3). In particular, the clear difference between the spherulite and the loosely packed crystal indicate different materials crystallizing sequentially.

Similar to SFW, the cooling scan of BW-oleogels shows a clear peak with a trailing shoulder. In this case short and irregular curved particles could be observed as initial solids (Event 1). Further cooling led to the development of curved, small feathery-like particles (Event 2) growing on the surface of existing solids.

The hydrolyzed variant of BW, BWh, shows multiple crystallization events in the DSC scan. The occurrence of distinct crystallization phenomena can be observed during the imaging operation as shown in the events 1 to 5 and can be directly linked to the DSC peaks.

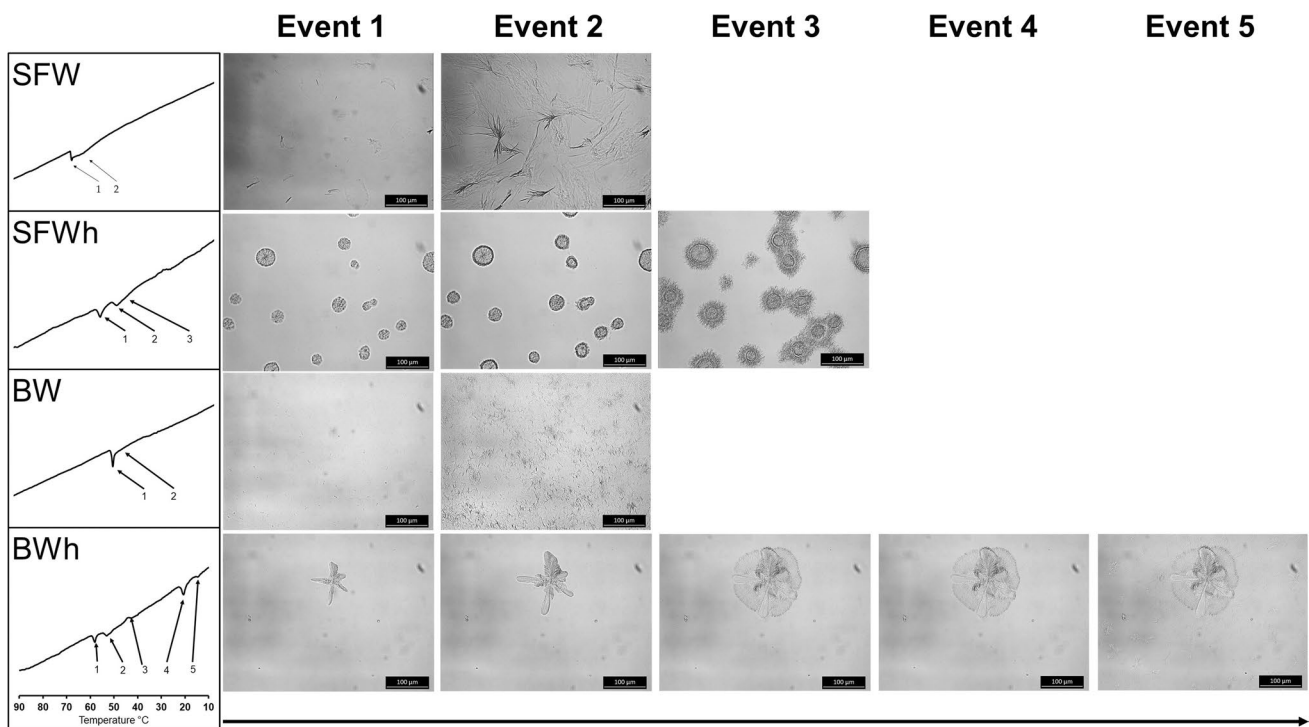


Fig. 6 Observable crystallization events during cooling in temperature scans at 0.1 °C/min during continuous imaging at a 200× magnification. Here, only the progress of the initial waxes (SFW, SFWh,

BW, BWWh) is depicted as temperature decreases (arrow = direction of cooling). The contrast was enhanced to better visualize structures

Figures 7 and 8 illustrate how composition and cooling affect the microstructure as observed by light microscopy. At the two higher cooling rates it can be observed that the basic structure of the agglomerates remains very similar. In line with the assumption that higher cooling rates favor nucleation, the size of the aggregates decreases and the number of particles increases with higher cooling rates. The magnitude of this effect, which is superimposed by different levels of aggregation, appears to be a function of the wax composition.

Regarding SFW-mixtures at very slow cooling (0.1 K/min), big and spherulitic aggregates shown for SFWh (Fig. 6) do not propagate into gels with mixed structuring systems based on either SFW or BW. When combining SFWh with BWWh, this morphology appears also in mixtures crystallized at low cooling rates. As the series of micrographs illustrates, the crystal morphology (either crystals or crystal aggregates) changes with both cooling rate and composition in a rather systematic manner. The effect of composition is most evident at low cooling rates. The micrographs of the BW-based systems reveal only a few structural elements. Including the data given in Fig. 2, these structures are most likely due to the mismatch of the resolution of the microscope and the crystal size and not an effect of excessive dissolution.

Firmness Measurement of Cooling Rate Treated Oleogels

Firmness is one of the most important criteria for the characterization of semi-solid fat phases. Currently, mainly rheological investigations are used in the assessment of differently cooled oleogels [25–27]. This seems to be appropriate whenever the structure efficiency of the investigated system is low and the applied rates are neither extremely low nor very high. This is confirmed by weak correlation of firmness data gathered by the different methods (data not shown). Nevertheless, the rheological measurements mostly characterize a sample not sufficiently stabilized. More extended considerations of this topic can be found elsewhere [16]. Alternatively, the firmness of a gel is determined by back extrusion. Here a gauge head is driven into the sample causing the gel to flow through the circular slit around the probe head [28]. Despite being prone to wall effects, the resulting signal is a combination of deformation and resistance against flow.

Considering these constraints, a new method to assess gel firmness/structure was developed. The extrusion and compression as described above is sensitive within a wider range of consistencies and yields additional information. Figure 9A shows the setup used for the extrusion out of the

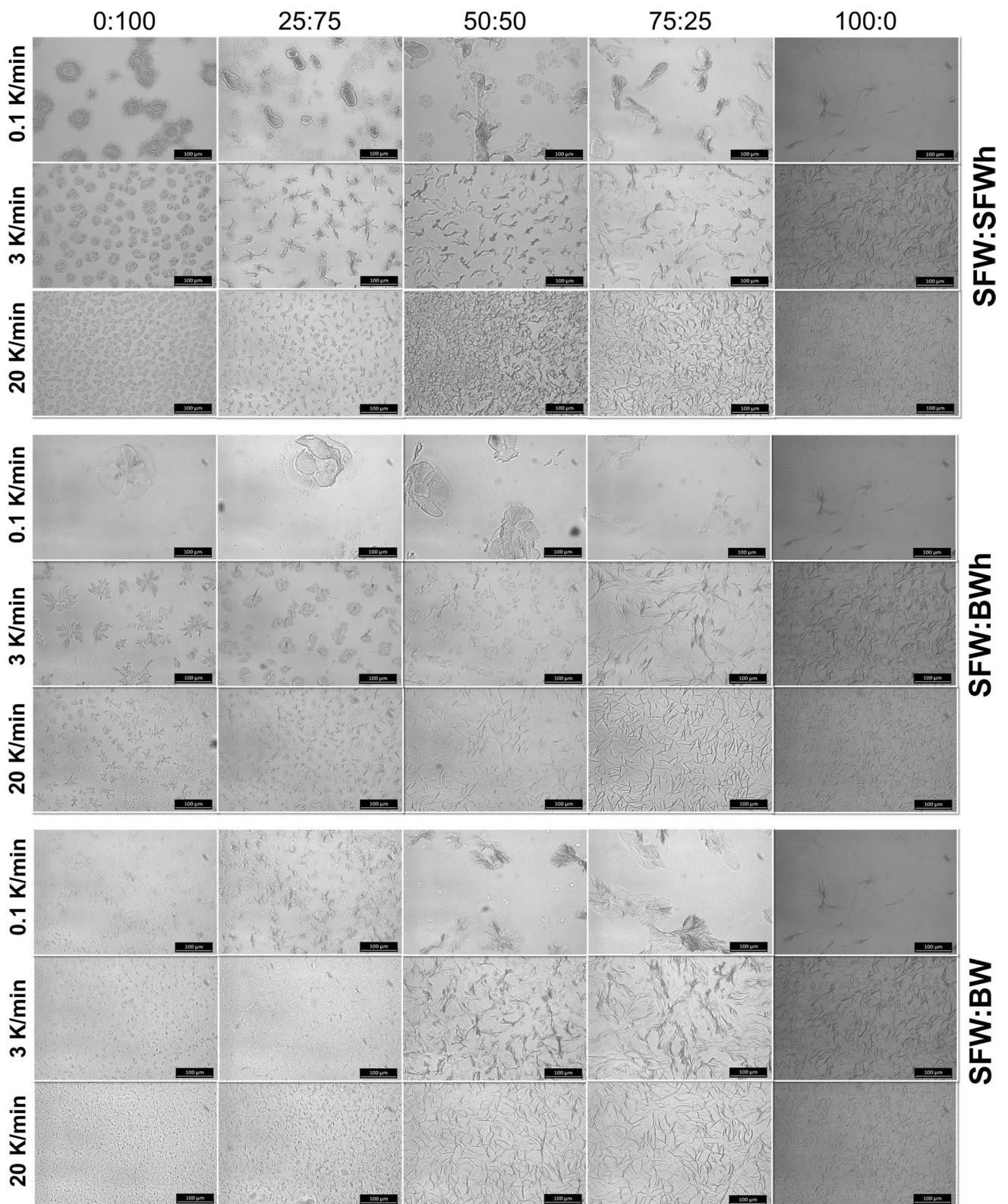


Fig. 7 Micrographs of 12% w/w oleogels produced with SFW-mixtures at 200 \times magnification after being crystallized at specified rates ($T = 15^{\circ}\text{C}$)

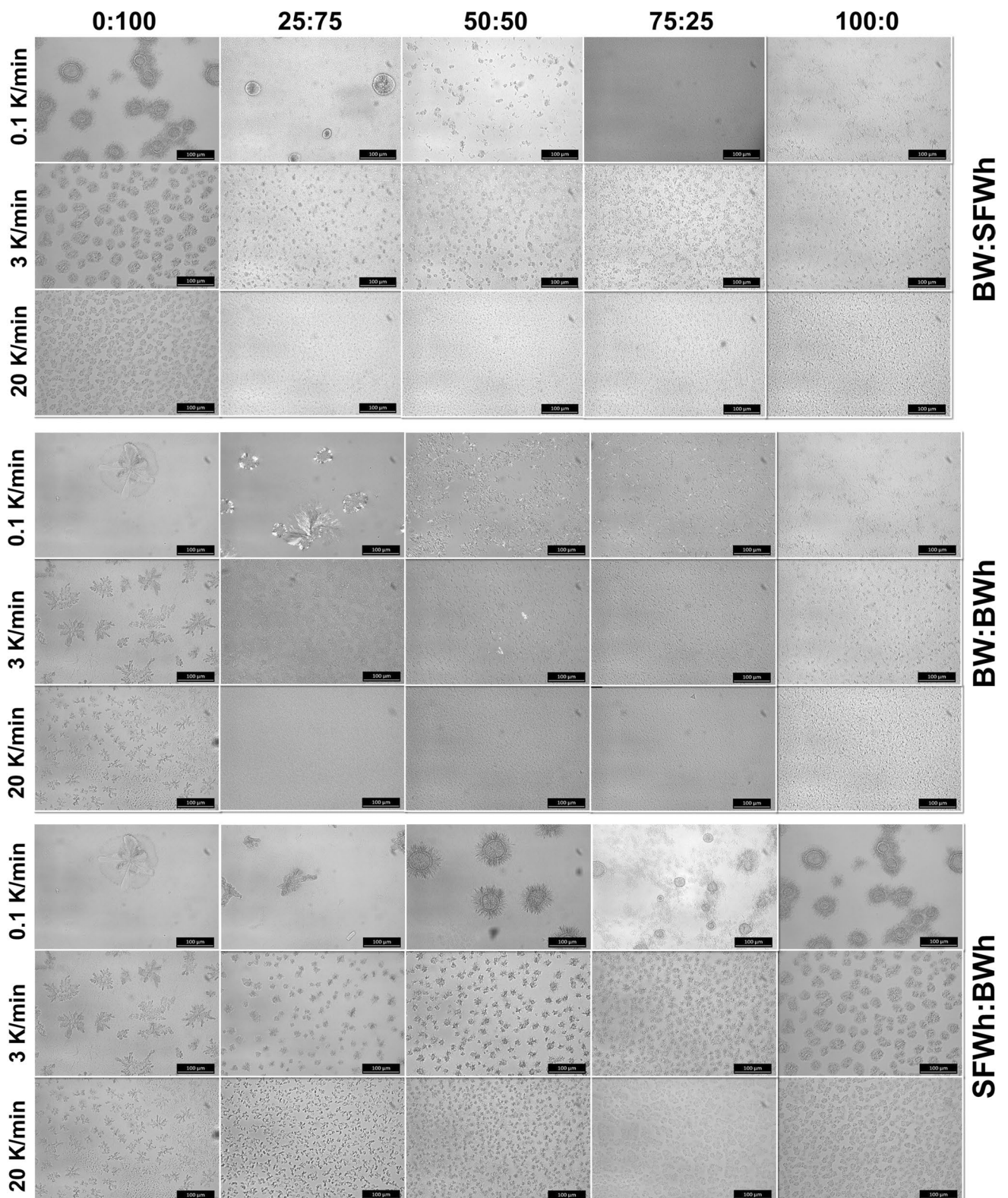


Fig. 8 Micrographs of 12% w/w oleogels produced with BW-mixtures and SFWh at 200× magnification after being crystallized at different rates ($T = 15\text{ }^{\circ}\text{C}$)

decapitated sample container. Applying a defined velocity and simultaneously monitoring the force necessary to move the gel plug, yields in characteristic values related to establish lubrication and maintenance of movement (Fig. 9C). The data show that the force necessary to move the gel plug through the tube is not scaling with reduced contact area between the gel plug and the wall. However, as soon as the gel plug is pushed forward, a thin gel film forms between the cylindrical probe head and the wall during extrusion. This ‘constant’ force necessary to establish a lubricating film either between the cylinders’ wall and the gel plug (or the cylinders’ wall and probe head) is an additional indication for the integrity of the gel plug. This was already found in preliminary tests during the method development. The subsequent compression test on the extruded samples (gel plugs) is consequently free of any wall effects. Figure 9B shows the F/l-curve for two different gels (16% w/w of either SFW or SFW_h). The substantial differences found, correspond somehow to the rheological results obtained for gels with these structurants earlier [16]. From the curve displayed in Fig. 9B, the value of the peak prior to structure breakdown is considered as firmness in this contribution which is also indicated by arrows. Figure 9D illustrates the quality of this firmness assessment compared to penetration measurements in petri dishes of the same samples. Actually 50 measurements of 16% w/w SFW oleogels were performed with each

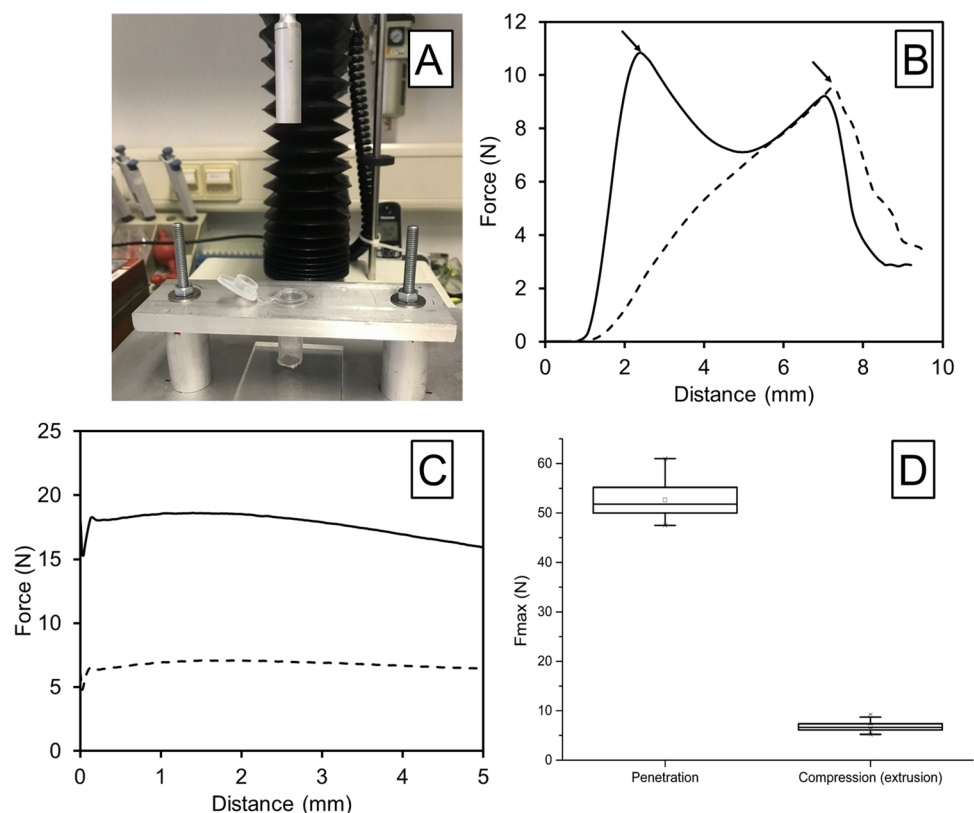
method. Admittedly, the relative deviation of 6.3% (± 3.3 N) for the penetration is better than the 13.05% (± 0.88 N) for the compression test. Nevertheless, the reproducibility of the new test appears acceptable while the data shown in Fig. 9B and C illustrate that characteristic information on the oleogels can be derived.

The evolution of the detected compression force as a function of the distance of the probe head is exemplarily depicted in Fig. 10 for the straight waxes. The data reveal that there is a clear effect of cooling rate on the structure of the gel.

As already established, SFW behaves differently than the other structuring agents. In line with earlier rheological findings [16], a first structure breakdown is observed at relatively small deformations corresponding to a limited extension of the linear viscoelastic region. This again is thought to be an indication for the link of SFW’ structure efficiency to sintering. Attempts to correlate the necessary detachment force ($F_{\max, \text{extrusion}}$) upon extrusion of the oleogels (compare Fig. 9C) with other gel characteristics were not successful. The determined values can be found elsewhere (SI 4). The data gathered from compression tests of the 16% w/w oleogels are processed as described above and displayed in Fig. 11.

The graphs for the different structuring systems illustrate consistently that the hardness increases with increasing cooling rate. This is not only in line with general expectations

Fig. 9 **A:** Setup of sample extrusion for firmness measurements. **B:** Compression force on extruded sample. All samples crystallized at 20 °C for 48 h in respectively containers; solid lines 16% w/w SFW oleogel, dashed lines: 16% w/w SFW_h oleogel. **C:** Force during extrusion (SFW, SFW_h) **D:** Comparison of 16% w/w SFW oleogels in penetration tests in petri dishes (left) and new extrusion-compression method (right) as boxplots ($n=50$ respectively)



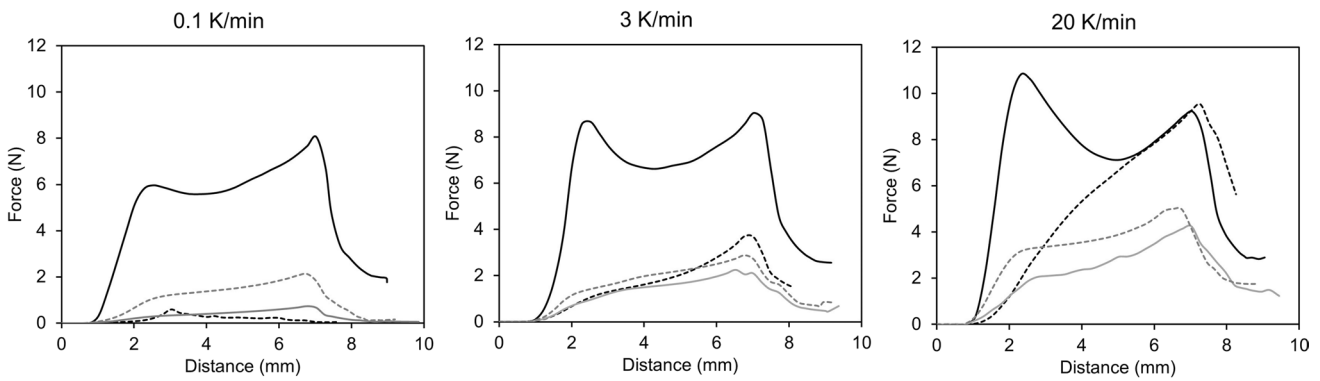


Fig. 10 Force-distance graphs of the compression tests of 16% w/w oleogels of straight structurants treated with different cooling rates. Solid black = SFW, dashed black = SFWh, solid grey = BW, dashed grey = BWh

relating to nucleation and growth kinetics but also corresponds to the micrographs given in Figs. 8 and 9. How strong the effect of the cooling rate is, depends on the

particular wax composition. The reduction from the highest and lowest firmness value on cooling rate reduction from 20 K/min to 0.1 K/min is approximately 25% in SFW-gels, 85%

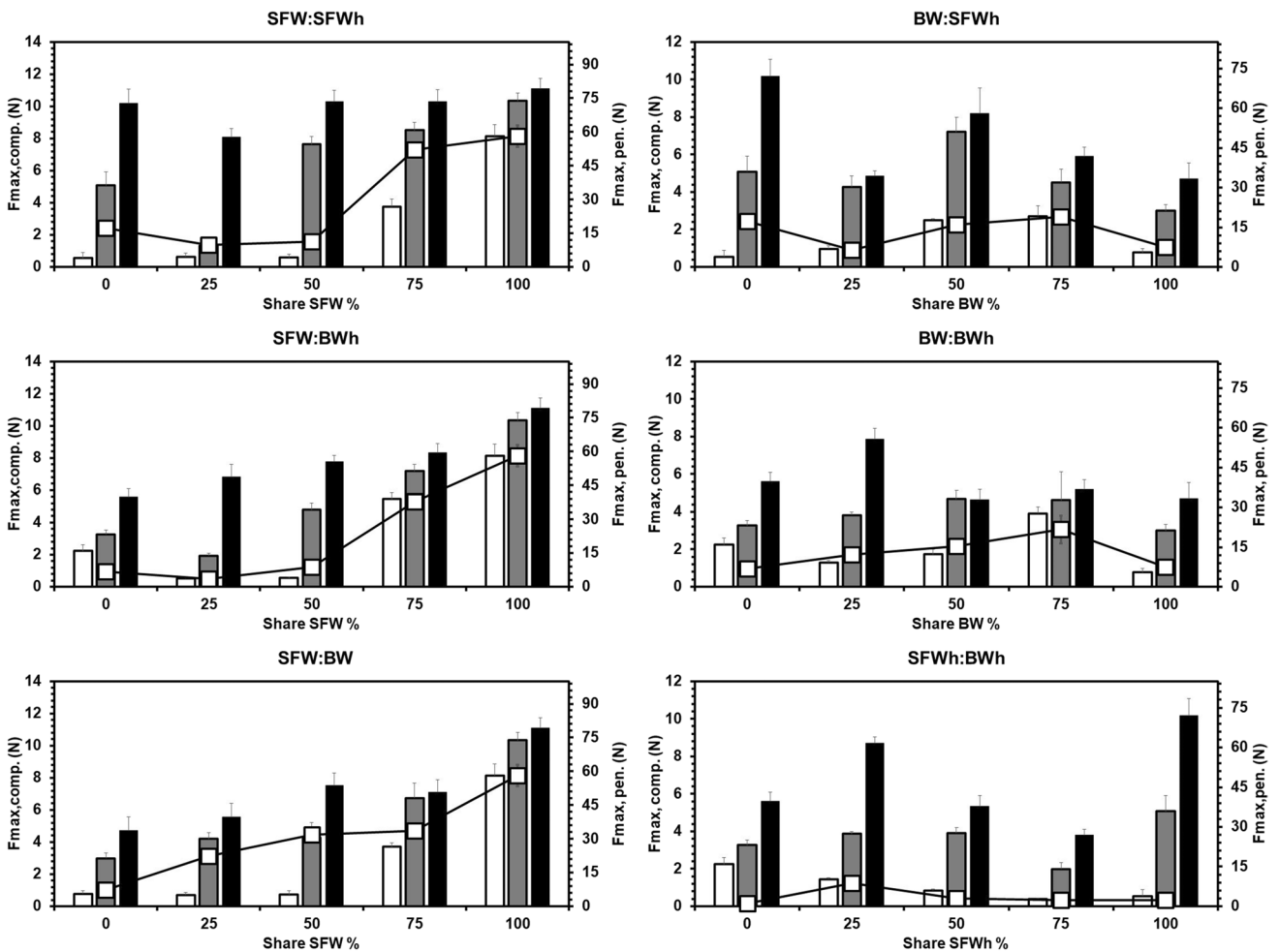


Fig. 11 Firmness values (F_{max}) of 16% w/w oleogels crystallized under rates of 0.1 K/min (white pillars), 3 K/min (grey pillars) and 20 K/min (black pillars) as a function of the share of component A in bi-wax mixtures (A:B). Squares (\square) refer to corresponding penetra-

tion tests (petri dishes) of the same waxes at an inclusion level of 16% w/w after cooling at 1.6 K/min and 48 h of stabilization, right y-axis. Scaling of both y-axis aligned according to Fig. 2D

for BW-gels, 95% for SFWh-gels and 65% for BWh-gels. The maximum firmness values determined by compression tests for a cooling rate of 20 K/min are: SFW 11.10 ± 0.6 N, BW 4.7 ± 0.8 N, SFWh 10.2 ± 0.8 N and BWh 5.6 ± 0.5 N. Considering the mixed structuring systems, it is found that in mixed systems containing SFW, SFW contributes the most to the structure irrespective of the cooling rate. Consequently, higher inclusion levels of SFW result in higher hardness values. When structuring with mixtures of SFW and SFWh, gels produced with the highest cooling rate (20 K/min) do not obey this trend. In this case the hardness appears to be almost independent of the wax composition. Only the structurant mixture 25:75 SFW:SFWh yields significantly lower values. The peculiar performance of mixtures containing 75% SFWh in the structurant phase is also expressed in the other systems. In combination with BW and BWh, SFWh gelled at 20 K/min with this inclusion level (75%) results in lowest firmness values as well. In contrast to this, BWh appears to deliver harder gels when constituting of 75% of the structurant mixture. These tendencies of gel hardness evolution as a function mixing structurants is in general also found back at the lower cooling rates. However, this is expressed much less clearly. Next to the hardness data gathered with the compression test, also hardness data on the same structurant systems (16% w/w) obtained by penetration tests are illustrated. The hardness values are taken by penetration tests in petri dishes, see also Fig. 9D. Samples were cooled quiescently at a rate of approximately 1.6 K/min. The data gathered from penetration tests (\square) are depicted against the y-axis on the right. This y-axis is scaled to the primary y-axis on the basis of the data displayed in Fig. 9D (7:1). Taking into account that the cooling rate is between 0.1 and 3 K/min (1.6 K/min) the agreement with the data presented here is stunning. These findings support the trends found as a function of mixing.

The results illustrate the importance of the SFW-WE in network formation, which is shown to be quite irrespective of the applied cooling rate. For all other mixtures the evolution of hardness as a function of mixture composition is more complex. With significant but variable amounts of FA, FaOH and HC present unravelling the respective contributions is beyond the scope of this contribution. These components could influence aggregation of primary crystals, act as crystal habit modifier, or build up additional solid phases. Apparently, these various contributions are also modified by the cooling rate upon gel formation. This interpretation is in line with Talbot et al. [29], who reported reduced crystal modification effects by minor components with increasing undercooling. Furthermore, chemical similarity of major and minor components was considered as important for strong interactions. The latter is obviously given for the systems studied since all species contain long aliphatic chains.

Conclusion

Oleogels based on different wax structurant systems were produced by applying significantly different cooling rates, 0.1, 3 and 20 K/min. Structuring systems dosed at 16% w/w level were pure and binary mixtures of sunflower wax, bees wax, and their respective hydrolyzates. In order to adequately characterize the samples, a new method to assess the hardness of gels was introduced. This was basically achieved by compression of extruded gel plugs. The data gathered reveal that the systems studied are strongly affected by cooling rate variations. For all samples, it was observed that the highest cooling rates result in the hardest gels. The sensitivity of gels' hardness varies significantly between the different structurant mixtures. It appears that within the range of variations (wax composition and cooling rate) cooling rate most strongly influences the gels' hardness.

The solubilities of the different structurant systems were derived from DSC data. It was found that most homogeneous waxes and wax mixtures show lowest solubilities which ranged between 0.5 and 3.5% w/w. Currently, these solubility data do not appear to provide an explanation for the obtained hardness values. Further processing of the data reveals that the heat of dissolution for each system does not vary as a function of cooling rate. This indicates no change of the type of solid material, either polymorphic form or co-crystallization. However, the thermograms on cooling and heating do vary for the different cooling rates. Compared to the higher crystallization temperatures and the sharper peaks at slow cooling, the observed higher dissolution temperatures for the slowly crystallized samples deserve further attention. The DSC data also allowed to compute the undercooling as a function of the degree of homogeneity (DoH) as defined in an earlier contribution of ours on different waxes. The data show that this concept applies also reasonably well to the systems studied. The micrographs essentially illustrate the expected trends resulting from changes in the applied cooling rate.

The significant differences found in this study emphasize that any application of wax-based oleogels requires a detailed understanding of the thermal processes involved in food production processes.

Supplementary Information The online version contains supplementary material available at <https://doi.org/10.1007/s11483-022-09725-y>.

Acknowledgements This IGF project AiF 20285 N of the FEI is/was supported via AiF within the programme for promoting the Industrial Collective Research (IGF) of the Federal Ministry of Economic Affairs and Climate Action (BMWK), based on a resolution of the German Parliament. The authors would like to express appreciation to Vivien Schreiber for the excellent and precise work.

Funding Open Access funding enabled and organized by Projekt DEAL. This research has been funded by cooperative industrial research of the German Federation of Industrial Research Associations (AiF) and cooperative industrial research (FEI) (AiF 20285 N).

Declarations

Conflict of Interest There are no conflicts to declare.

Open Access This article is licensed under a Creative Commons Attribution 4.0 International License, which permits use, sharing, adaptation, distribution and reproduction in any medium or format, as long as you give appropriate credit to the original author(s) and the source, provide a link to the Creative Commons licence, and indicate if changes were made. The images or other third party material in this article are included in the article's Creative Commons licence, unless indicated otherwise in a credit line to the material. If material is not included in the article's Creative Commons licence and your intended use is not permitted by statutory regulation or exceeds the permitted use, you will need to obtain permission directly from the copyright holder. To view a copy of this licence, visit <http://creativecommons.org/licenses/by/4.0/>.

References

1. M.A. Briggs, K.S. Petersen, P.M. Kris-Etherton, *Healthcare*. **5**(2) (2017). <https://doi.org/10.3390/healthcare5020029>
2. G.P. Zaloga, K.A. Harvey, W. Stillwell, R. Siddiqui, *Nutr. Clin. Pract.* **21**(5), 505–512 (2006).
3. C.D. Doan, I. Tavernier, P.K. Okuro, K. Dewettinck, *Innov. Food. Sci. Emerg. Technol.* **45**, 42–52 (2018).
4. M. Scharfe, E. Flöter, *Eur. J. Lipid. Sci. Technol.* **122**(12), 2000213 (2020).
5. G. Avendaño-Vásquez, A. de La Peña-Gil, M.E. Charó-Alvarado, M.A. Charó-Alonso, J.F. Toro-Vazquez, *Front. Sustain. Food. Syst.* **4**, 352 (2020).
6. D.J. Abdallah, L. Lu, R.G. Weiss, *Chem. Mater.* **11**(10), 2907–2911 (1999).
7. F.G. Gandolfo, A. Bot, E. Flöter, *JAACS*. **2004**(81), 1–6 (2004).
8. C.D. Doan, C.M. To, M.D. Vrieze, F. Lynen, S. Danthine, A. Brown, K. Dewettinck, A.R. Patel, *Food. Chem.* **214**(214), 717–725 (2017).
9. M. Scharfe, J. Niksch, E. Flöter, *Eur. J. Lipid. Sci. Technol.* (2021)
10. T. Wettlaufer, H. Brykczynski, E. Flöter, *Eur. J. Lipid. Sci. Technol.* (2021). <https://doi.org/10.1002/ejlt.202100114>
11. A.I. Blake, A.G. Marangoni, *Food. Biophys.* **10**(4), 456–465 (2015).
12. A.I. Blake, A.G. Marangoni, *Food. Biophys.* **10**(4), 403–415 (2015).
13. A.I. Blake, E.D. Co, A.G. Marangoni, *J. Am. Oil. Chem. Soc.* **91**(6), 885–903 (2014).
14. Y. Yao, H. Zhou, W. Liu, C. Li, S. Wang, *J. Oleo. Sci.* **70**(1), 135–143 (2021).
15. M. Callau, K. Sow-Kébé, L. Nicolas-Morgantini, A.-L. Fameau, *J. Colloid. Interface. Sci.* **560**(560), 874–884 (2019).
16. T. Wettlaufer, B. Hetzer, E. Flöter, *Eur. J. Lipid. Sci. Technol.* **123**(7), 2000345 (2021).
17. E. Flöter, M. Haeupler, K. Sato, in *Crystallization of lipids*. ed. by K. Satō (Wiley, Hoboken, NJ, USA, 2018), pp. 61–104
18. C. Blach, A.J. Gravelle, F. Peyrone, J. Weiss, S. Barbut, A.G. Marangoni, *RSC. Adv.* **2016**(6), 81151 (2016).
19. H.M. Schaink, K.F. van Malssen, S. Morgado-Alves, D. Kalnin, E. van der Linden, *Food. Res. Int.* **40**(9), 1185–1193 (2007).
20. J. Los, E. Flöter, *Phys. Chem. Chem. Phys.* **1**, 4251–4257 (1999)
21. A.I. Blake, A.G. Marangoni, *Food. Struct.* **3**, 30–34 (2015).
22. H.-S. Hwang, S. Kim, K.O. Evans, C. Koga, Y. Lee, *Food. Struct.* **5**(5), 10–20 (2015).
23. H. Brykczynski, *Wax-based oleogels - characterization and re-engineering of waxes* (Berlin, 2021)
24. K. Sato, (ed.), *Crystallization of lipids*, 1st edn. (John Wiley & Sons Ltd, West Sussex, 2018)
25. A. de La Peña-Gil, F.M. Álvarez-Mitre, M.M. González-Chávez, M.A. Charó-Alonso, J.F. Toro-Vazquez, *Food. Res. Int. (Ottawa, Ont.)* **93**, 52–65 (2017). <https://doi.org/10.1016/j.foodres.2017.01.010>
26. M. Davidovich-Pinhas, S. Barbut, A.G. Marangoni, *Carbohydr. Polym.* **117**, 869–878 (2015).
27. J.A. Morales-Rueda, E. Dibildox-Alvarado, M.A. Charó-Alonso, R.G. Weiss, J.F. Toro-Vazquez, *Eur. J. Lipid. Sci. Technol.* **111**(2), 207–215 (2009).
28. A.K. Zetzl, A.G. Marangoni, S. Barbut, *Food. Funct.* **3**(3), 327–337 (2012).
29. G. Talbot, K. Smith, K. Bhaggan, *Lipid. Technol.* **24**(4), 83–85 (2012).

Publisher's Note Springer Nature remains neutral with regard to jurisdictional claims in published maps and institutional affiliations.